International Journal of Biological Macromolecules 283 (2024) 137604

Contents lists available at ScienceDirect

International Journal of Biological Macromolecules

journal homepage: www.elsevier.com/locate/ijbiomac

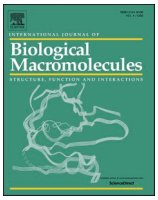

Two pairs of back-to-back α-helices of *Kingella kingae* RtxA toxin are crucial for the formation of a membrane pore

Eliska Ruzickova [a,b,1], Michaela Lichvarova [a,b,1], Adriana Osickova [a,1], Katerina Filipi [a], David Jurnecka [a], Humaira Khaliq [a,c], Carlos Espinosa-Vinals [a,c], Petr Pompach [d], Jiri Masin [a], Radim Osicka [a,*]

[a] Institute of Microbiology of the Czech Academy of Sciences, Prague, Czech Republic
[b] Faculty of Science, Charles University, Prague, Czech Republic
[c] University of Chemistry and Technology, Prague, Prague, Czech Republic
[d] Institute of Biotechnology of the Czech Academy of Sciences, Vestec, Czech Republic

ARTICLE INFO

Keywords:
Kingella kingae
Membrane topology
RtxA
Structure-function

ABSTRACT

The RtxA cytotoxin, a member of the RTX (Repeats in ToXin) family of pore-forming toxins, is the primary virulence factor of the paediatric facultative pathogen *Kingella kingae*. Although structure-function studies of RTX toxins have defined their characteristic domains and features, the exact membrane topology of RTX toxins remains unknown. Here, we used labelling of cell-bound RtxA with a membrane-impermeable, lysine-reactive reagent and subsequent detection of the labelled lysine residues by mass spectrometry, which revealed that most of the membrane-bound toxin is localised extracellularly. A trypsin protection assay with cell-bound RtxA demonstrated that five of seven transmembrane α-helices, predicted by various algorithms within the N-terminal half of the molecule, are irreversibly embedded in the membrane. Structure-function analysis showed that these α-helices, four of which are arranged as two pairs of back-to-back helices, are essential for the formation of an ion-conducting membrane pore. In contrast, the C-terminal half of RtxA is required for the interaction with the cell surface and for the irreversible insertion of the toxin into the membrane via acyl chains covalently linked to the molecule. These findings advance our understanding of the structure-function relationships of RtxA and enable us to propose a membrane topology model of the toxin.

1. Introduction

The Gram-negative coccobacillus *Kingella kingae*, which until recently was thought to cause infections only rarely, is now considered to be a significant paediatric pathogen [1–5]. It normally occurs as part of the oropharyngeal microbiota of young children as a commensal microorganism. However, when the bacteria cross the epithelial barrier and spread throughout the body, they can cause serious infections such as osteomyelitis, septic arthritis, occult bacteraemia, endocarditis or pneumonia [2,3,6]. Children with the highest rate of oropharyngeal *K. kingae* colonization and invasive infections are aged between 6 and 36 months, with the musculoskeletal system being the most commonly affected part of the body [7–10]. *K. kingae* virulence factors include type IV pili, a trimeric autotransporter adhesin Knh, a polysaccharide capsule, a galactan exopolysaccharide and an RtxA cytotoxin, which belongs to the family of RTX (Repeats in ToXin) toxins secreted by various Gram-negative pathogens [11–16].

Based on primary sequence homology with other RTX toxins [16–18] and an AlphaFold model [19,20], several distinct regions can be predicted in the 956 residues-long polypeptide of RtxA (Fig. 1A and B): (i) an N-terminal segment of unknown function; (ii) a hydrophobic domain (residues 130 to 430) with several predicted transmembrane α-helical segments, which are presumably responsible for the pore-forming activity of the toxin; (iii) an acylated segment (residues 510 to 725) in which activation of the proRtxA protoxin to the active RtxA toxin occurs by the co-expressed acyltransferase RtxC, which catalyses the acylation of two conserved lysine residues (K558 and K689) [21,22]; (iv) a typical calcium-binding RTX domain (residues 725 to 815), which harbours the conserved nonapeptide repeat sequences that form calcium-binding sites; and (v) a C-proximal secretion signal that enables export of the

* Corresponding author.
E-mail address: osicka@biomed.cas.cz (R. Osicka).
[1] These authors contributed equally to this work.

https://doi.org/10.1016/j.ijbiomac.2024.137604
Received 27 September 2024; Received in revised form 1 November 2024; Accepted 11 November 2024
Available online 13 November 2024

toxin through the bacterial envelope via the type 1 secretion system.

After secretion, RtxA recognises negatively charged sialic acid residues on the surface of host cells that are covalently bound to various glycosylated cell surface structures, such as glycoproteins and gangliosides [23,24]. The interaction of RtxA with the host cell surface is further enhanced by membrane cholesterol, which directly interacts with the toxin [21]. Interestingly, unlike some other RTX toxins, RtxA does not interact with leukocyte-restricted β_2 integrins as specific cell receptors [23]. After binding, RtxA inserts into the cell membrane and forms cation-selective pores that trigger cation fluxes across the cell membrane, leading to disruption of normal cell physiology and ultimately cell death [21,25]. Indeed, several studies have shown that RtxA is cytotoxic to various eukaryotic cells, such as human laryngeal HlaC-78 squamous cells, hypopharyngeal FaDu epithelial cells, synovial SW 982 cells, bone osteosarcoma U-2 OS epithelial cells, monocyte/macrophage RAW 264.7 cells and monocytic THP-1 cells [11,21,26]. As genes for the production, activation and secretion of RtxA are present in all clinical isolates causing invasive *K. kingae* diseases and intraperitoneal infection of an infant rat with an RtxA-deficient mutant strain resulted in less histopathological changes than infection with a wild-type strain, it is believed that RtxA is the main virulence factor of *K. kingae* [27–30]. Recently, it was also shown that a duplication of the *rtxA* gene, encoding the RtxA toxin, is associated with invasive *K. kingae* diseases and in vitro experiments with isogenic strains revealed that two copies of the *rtxA* gene are associated with increased virulence of *K. kingae* compared to a single copy [31].

Although *K. kingae* is recognised as an emerging paediatric pathogen and RtxA is its key virulence factor, the structure-function relationships and membrane topology of the toxin are unknown. In this study, we employed a combination of bioinformatic prediction tools, biophysical approaches and biochemical methods to elucidate the membrane topology of RtxA, characterise the role of individual regions of the toxin in its binding and cytolytic activity and identify the transmembrane segments involved in the formation of an ion-conducting membrane pore.

2. Materials and methods

2.1. Bacterial strains

The *Escherichia coli* strain XL1-Blue (Stratagene, La Jolla, CA, USA), used for DNA manipulations, was cultured in Luria-Bertani medium at 37 °C. The *E. coli* strain BL21 (Novagen, Madison, WI, USA), transformed with the plasmid pMM100 (encoding LacI and tetracycline resistance), was used for the expression of intact RtxA and its mutant variants.

2.2. Plasmids and plasmid construction

The plasmid pT7*rtxA* was used to produce unacylated proRtxA protoxin, while the plasmid pT7*rtxC-rtxA* was used to produce RtxC-acylated RtxA toxin [21]. Oligonucleotide-directed PCR mutagenesis was used to construct plasmids derived from pT7*rtxC-rtxA* for the expression of RtxC-acylated RtxA variants with specific deletions and single amino acid substitutions. The presence of the desired deletions and substitutions, as well as the absence of unintended mutations, were verified by sequencing (Eurofins Genomics, Ebersberg, Germany). All RtxA variants and proRtxA contain a C-terminal double-hexahistidine tag for affinity purification on Ni-NTA beads [32].

2.3. Protein production and purification

Intact RtxA, unacylated proRtxA and RtxA mutants were produced in *E. coli* BL21/pMM100 cells and purified under denaturing conditions in urea by a combination of affinity chromatography on an Ni-NTA agarose column (Qiagen, Germantown, MD, USA) and hydrophobic chromatography on a Phenyl-Sepharose CL-4B column (Sigma–Aldrich, St. Louis, MO, USA) as previously described [21].

2.4. Sheep erythrocytes

Sheep erythrocytes (LabMediaServis, Jaromer, Czech Republic) were

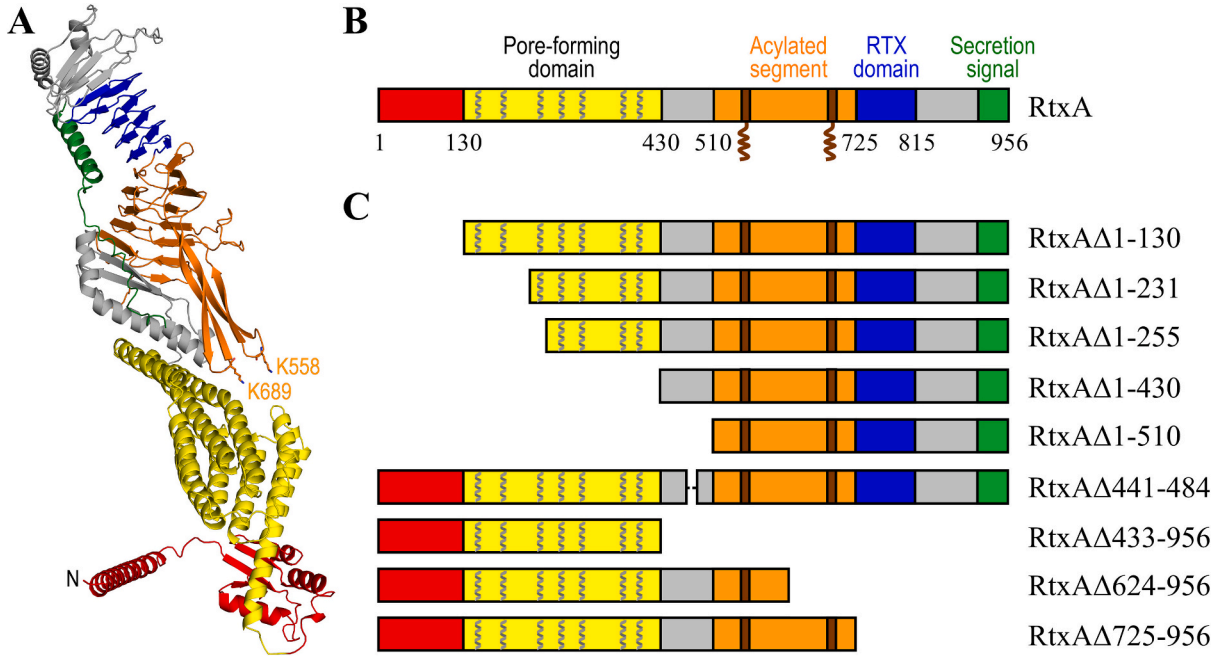

Fig. 1. AlphaFold model and schematic representation of RtxA and its deletion variants. **(A)** AlphaFold structure prediction of RtxA (UniProt number: A0A1X7QMH9) adapted from the AlphaFold Protein Structure Database [19,20]. **(B)** Schematic representation of RtxA showing the N-terminal segment (red), the pore-forming domain (yellow) with seven predicted transmembrane α-helical segments, the acylated segment (orange) with two acylated lysine residues (K558 and K689), the calcium-binding RTX domain (blue) and the C-terminal secretion signal (green). The colour coding corresponds to the AlphaFold model shown in panel (A). **(C)** Deletion mutants of RtxA used in this study.

supplied in Alsever's Solution (Sigma–Aldrich, St. Louis, MO, USA). Prior to each experiment, the erythrocytes were washed three times with TNC buffer (50 mM Tris-HCl (pH 7.4), 150 mM NaCl and 2 mM $CaCl_2$) and then resuspended in a desired buffer to achieve the required cell density.

2.5. Binding assay

Washed erythrocytes (2×10^6) in 200 μl of TNC buffer supplemented with 100 mM polyethylene glycol (PEG) 1500 (TNC/PEG) were incubated with various concentrations (0–38 nM) of RtxA, proRtxA or RtxA mutants for 15 min at 22 °C. Unbound toxin molecules were removed by washing with 100 mM sodium carbonate (pH 10.5) supplemented with PEG 1500, followed by washing with TNC/PEG supplemented with 1 % fetal calf serum (FCS). The toxin molecules bound to the erythrocytes were then labelled for 15 min at 4 °C with a 6 × His Tag monoclonal antibody conjugated to Alexa Fluor 488 (Thermo Fisher Scientific, Waltham, MA, USA) diluted 1:500 in TNC/PEG supplemented with 1 % FCS. After labelling, the erythrocytes were washed twice with TNC/PEG and the amount of the cell-bound toxin molecules was quantified by flow cytometry using a FACS LSR II instrument (BD Biosciences, San Jose, CA, USA). Data were analysed using FlowJo software (Tree Star, Ashland, OR, USA) and appropriate gating was used to exclude cell aggregates and debris. Binding data were deduced from the median fluorescence intensity (MFI) of the bound RtxA variants and expressed as the percentage of intact RtxA binding to erythrocytes at a concentration of 38 nM (taken as 100 %).

2.6. Haemoglobin release assay

Washed erythrocytes (5×10^8) in 1 ml of either TNC buffer or TNC buffer supplemented with 100 mM osmoprotectant (saccharose, maltose, or PEG with an average molecular weight of 400, 1000, 1500, 2000 or 3000 g/mol) were incubated with various concentrations of RtxA, proRtxA or RtxA mutants. Haemolytic activity was measured in time by photometric determination (A_{541}) of the haemoglobin release [21].

2.7. Sulfo-biotinylation of RtxA bound to erythrocytes

Washed erythrocytes (5×10^9) were resuspended in 10 ml of HNC buffer (50 mM HEPES (pH 7.4), 150 mM NaCl and 2 mM $CaCl_2$) supplemented with 100 mM PEG 1500 (HNC/PEG buffer), incubated with purified RtxA (30 μg/ml) for 15 min at 37 °C and then thoroughly washed with HNC/PEG buffer to remove the unbound RtxA molecules. The washed erythrocytes were then incubated in 1 ml of HNC/PEG buffer supplemented with 2 mM sulfo-NHS-LC-biotin (Thermo Fisher Scientific, Waltham, MA, USA) on a mini-rotator for 45 min at 22 °C. To quench and remove the unincorporated sulfo-biotin reagent, erythrocytes were washed with TNC/PEG buffer and the RtxA molecules only loosely associated with the erythrocyte membrane were stripped off with 100 mM alkaline sodium carbonate (pH 11.5). After washing with TNC/PEG buffer, erythrocytes were resuspended in 1 ml of HNC buffer containing protease inhibitors (cOmplete™, Mini, EDTA-free Protease Inhibitor Cocktail; Roche, Basel, Switzerland). In the HNC buffer, lacking PEG 1500 as an osmoprotectant, the RtxA molecules inserted into the cell membranes immediately caused erythrocyte lysis. The erythrocyte membranes were pelleted by centrifugation (16,000 *g*, 5 min, 4 °C) and solubilised with 1 ml of TNT buffer (50 mM Tris-HCl (pH 7.4), 150 mM NaCl, 1 % Triton X-100 and EDTA-free Protease Inhibitor Cocktail) on a mini-rotator for 30 min at 4 °C. The sample was clarified by centrifugation (16,000 *g*, 15 min, 4 °C) and the resulting supernatant containing RtxA was mixed with 300 μl of Ni-NTA Sepharose beads, which were previously washed with equilibration buffer (50 mM Tris-HCl (pH 7.4), 300 mM NaCl). After 1 h of incubation on a mini-rotator at 4 °C, the beads were thoroughly washed with washing buffer (50 mM Tris-HCl (pH 7.4), 300 mM NaCl, 30 mM imidazole) and the biotinylated RtxA was eluted with 1 ml of elution buffer (50 mM phosphate buffer (pH 7.4), 300 mM NaCl, 250 mM imidazole) and analysed by mass spectrometry.

2.8. Preparation of cholesterol-containing liposomes

1-palmitoyl-2-oleoyl-sn-glycero-3-phosphocholine (POPC, Avanti Polar Lipids, Birmingham, AL, USA) and cholesterol (Sigma–Aldrich, St. Louis, MO, USA) at a ratio of 3:1 (w/w) were vigorously resuspended in chloroform, which was then evaporated with a slow stream of nitrogen. A thin, uniform lipid film formed on the sides of a round-bottom test tube was rehydrated in HNC buffer and liposomes were formed by vigorous shaking. The liposomes were then extruded through a Nucleopore Track-Etched Polycarbonate filter with a pore size of 1 μm (Whatman, 800281, GE Healthcare Bio-Sciences, Pittsburgh, PA, USA) using an Avanti Mini Extruder (Avanti Polar Lipids, Alabaster, AL, USA) with two 0.5 ml Hamilton syringes (Hamilton, Reno, NV, USA). The prepared liposomes were counted by flow cytometry using a FACS LSR II instrument (BD Biosciences, San Jose, CA, USA). Absolute liposome counting was achieved using Invitrogen CountBright Absolute Counting Beads (Thermo Fisher Scientific, Waltham, MA, USA), allowing precise enumeration of liposomes per volume.

2.9. Digestion of RtxA bound to erythrocytes and liposomes

Washed erythrocytes (5×10^9) were resuspended in 10 ml of HNC/PEG buffer and incubated with purified RtxA (30 μg/ml) for 15 min at 37 °C. To remove the unbound RtxA molecules, the erythrocytes were thoroughly washed with HNC/PEG buffer and then resuspended in HNE buffer (50 mM HEPES, 150 mM NaCl, 5 mM EDTA (pH 7.4)) supplemented with mass spectrometry grade trypsin (33 μg/ml). After 1 h at 37 °C, the erythrocyte membranes with trypsin-protected RtxA segments were gradually washed with HNE buffer, 100 mM sodium carbonate (pH 11.5) and HNE buffer, and finally resuspended in 50 μl of TU buffer (50 mM Tris-HCl (pH 7.4), 8 M urea).

Cholesterol-containing liposomes (1×10^6/ml) were incubated with purified RtxA (30 μg/ml) for 15 min at 37 °C, washed with HNC buffer and then resuspended in HNE buffer supplemented with mass spectrometry grade trypsin (22 μg/ml). After 1 h at 37 °C, the liposome membranes containing trypsin-protected RtxA segments were gradually washed with HNE buffer, 100 mM sodium carbonate (pH 11.5) and HNE buffer, and finally resuspended in 50 μl of TU buffer.

2.10. Liquid chromatography-tandem mass spectrometry analysis

The samples of sulfo-biotinylated RtxA were applied to a 30 kDa cutoff membrane filter and processed according to a modified protocol for filter-aided sample preparation [33]. Briefly, the samples were washed twice with AB buffer (50 mM ammonium bicarbonate (pH 8.3)) and mass spectrometry grade trypsin in AB buffer was added to the filter at a protein/enzyme ratio of 25:1. The samples were incubated overnight on a shaker at 37 °C and 200 rpm. The resulting peptides were eluted by three consecutive centrifugations with AB buffer at 14,000 *g* for 20 min, desalted using ZipTip pipette tips filled with C18 extraction disks (Thermo Fisher Scientific, Waltham, MA, USA) and vacuum dried. Prior to liquid chromatography-tandem mass spectrometry (LC-MS/MS) analysis, the samples were resuspended in 2 % acetonitrile (ACN), 0.1 % formic acid (FA).

The samples containing RtxA peptides were analysed using either a Vanquish liquid chromatography system (Thermo Scientific, Waltham, MA, USA) connected to the timsTOF SCP mass spectrometer (Bruker Daltonics, Billerica, MA, USA) or an Agilent 1290 liquid chromatography system (Agilent Technologies, Santa Clara, CA, USA) connected to the timsTOF Pro PASEF mass spectrometer (Bruker Daltonics, Billerica, MA, USA), both operating in a positive data-dependent mode. For

analysis with the timsTOF SCP system, 1 μl of the peptide mixture was injected onto the C18 trap column (Pepmap Neo C18, 5 μm, 0.3 × 5 mm; Thermo Scientific, Waltham, MA, USA) by an autosampler. After trapping, the peptides were eluted and separated on a C18 column (Pepsep C18, 150 × 0.15 mm, 1.5 μm; Bruker Daltonics, Billerica, MA, USA) using a linear 35-min water−ACN gradient from 5 % (v/v) to 35 % (v/v) ACN at a flow rate of 1.5 μl/min. For analysis with the timsTOF Pro system, 5 μl of the peptide mixture was injected onto the C18 trap column (UHPLC Fully Porous Polar C18, 0.3 × 20 mm; Phenomenex, Torrance, CA, USA) by an autosampler. After 5 min of trapping at a flow rate of 20 μl/min, the peptides were eluted and separated on a C18 column (Luna Omega 3 μm Polar C18, 100 Å, 150 × 0.3 mm; Phenomenex, Torrance, CA, USA) using a linear 35-min water−ACN gradient from 5 % (v/v) to 100 % (v/v) ACN at a flow rate of 4 μl/min. The mass spectrometers operated in data-dependent MS/MS mode using the standard proteomics PASEF method. The target intensity per individual PASEF precursor was set to 6000 and 20,000 for the timsTOF Pro and SCP, respectively. The intensity threshold was set to 1500. The scan range was set between 0.6 and 1.6 V·s/cm^2 with a ramp time of 100 ms and the number of PASEF MS/MS scans was set to 10. Precursor ions in the *m/z* range between 100 and 1700 with charge states ≥2+ and ≤6+ were selected for fragmentation. The active exclusion was enabled for 0.4 min.

The 50 μl samples of the trypsin-protected RtxA segments incorporated into the membranes of erythrocytes and liposomes were mixed with 50 μl of acidifying buffer (1 M glycine-HCl (pH 2.3)) and manually injected into the LC system using a PAL DHR autosampler (CTC Analytics AG, Zwingen, Switzerland) controlled by Chronos software (AxelSemrau, Sprockhövel, Germany). The LC system consisted of a temperature-controlled box and an Agilent Infinity II UPLC (Agilent Technologies, Santa Clara, CA, USA) connected directly to the ESI source of timsTOF Pro (Bruker Daltonics, Billerica, MA, USA). The injected sample was added onto a custom-made protease column packed with immobilised nepenthesin-2 and pepsin matrix (bed volume 66 μl) where the tryptic peptides were digested at 22 °C. The peptides were then loaded onto the trap column (SecurityGuard™ ULTRA Cartridge UHPLC Fully Porous Polar C18, 2.1 mm ID; Phenomenex, Torrance, CA, USA) under a flow of 0.4 % formic acid (FA) in water, driven by the 1260 Infinity II Quaternary pump at a flow rate of 200 μl/min. After 3 min, the desalted peptides were eluted and separated on an analytical column (Luna Omega Polar C18, 1.6 μm, 100 Å, 1.0 × 100 mm; Phenomenex, Torrance, CA, USA) under a water−ACN gradient (10 % (v/v) to 45 % (v/v) in 6 min; solvent A: 0.1 % FA in water, solvent B: 0.1 % FA, 2 % water in ACN). The water−ACN gradient was delivered by the 1290 Infinity II LC pump (Agilent Technologies, Santa Clara, CA, USA) at a flow rate of 50 μl/min.

The acquired LC-MS/MS data were searched against a customised database containing the modified sequence of RtxA (Uniprot: A1YKW7) using PeaksStudio 10.0 or 11.0 software (Bioinformatics Solutions Inc., Waterloo, Canada). The search parameters were set as follows: enzyme–trypsin (semi-specific)/nepenthesin-2 and pepsin matrix (non-specific), oxidation of methionine, precursor tolerance 15 ppm, fragment ion tolerance 0.05 Da and FDR < 1 %.

2.11. Circular dichroism spectroscopy

To determine the secondary structure of RtxA after its refolding, the circular dichroism (CD) spectra of RtxA proteins were acquired by CD spectroscopy. The RtxA, RtxAΔ1–510 and RtxAΔ433–956 proteins were concentrated by ultrafiltration to a final stock concentration of ~20 mg/ml using ultrafiltration units with a 10 kDa cutoff membrane (Millipore, Burlington, MA, USA). The concentrated, urea-unfolded RtxA variants were then refolded to a concentration of 0.2 mg/ml by rapid dilution in 20 mM Tris-HCl (pH 8.0), 50 mM NaCl with or without 2 mM $CaCl_2$. CD spectra of the proteins were measured in the wavelength range of 200–260 nm using a Suprasil 110-QS quartz cell with 0.1 cm path length (Hellma, Müllheim, Germany) and a Chirascan CD spectrometer (Applied Photophysics, Charlotte, NC, USA). Each protein was measured in two independent experiments with three accumulations per experiment to increase the signal/noise ratio. Ellipticities (mdeg) were converted to mean residue ellipticities (deg × cm^2 × dmol^{-1}).

2.12. Planar lipid bilayers

Measurements of RtxA variants on planar lipid bilayers were performed using Teflon cells separated by a diaphragm with a circular hole (diameter 0.5 mm) bearing the lipid membrane, as previously described [21,22,34]. Briefly, the membrane was formed by the painting method using soybean lecithin dissolved in n-decane–butanol (9:1 (v/v)). The RtxA variants were pre-diluted in TUC buffer (50 mM Tris-HCl (pH 8.0), 8 M urea and 2 mM $CaCl_2$) and added into the grounded cis compartment with a positive potential. Both compartments contained 150 mM KCl, 10 mM Tris-HCl (pH 7.4) and 2 mM $CaCl_2$. The membrane current was registered by Ag/AgCl electrodes with salt bridges at a voltage of 50 mV and a temperature of 22 °C. The signal was amplified by an LCA-200-10G amplifier (Femto, Berlin, Germany) and digitised using a LabQuest Mini A/D convertor (Vernier, Beaverton, OR, USA). All the signals were analysed by the QuB software [35].

2.13. Statistical analysis

Results are expressed as the arithmetic mean ± standard deviation (SD). Statistical analysis was performed using one-way or two-way ANOVA, followed by Dunnett's post-test, with GraphPad Prism 10.2.2 (GraphPad Software, La Jolla, CA, USA).

3. Results

3.1. Most of the cell-bound RtxA molecule is localised extracellularly

To detect extracellular parts of the cell-bound RtxA toxin, we have developed a new approach based on the labelling of the toxin with a membrane-impermeable, lysine-reactive reagent and the subsequent detection of the labelled lysine residues by LC-MS/MS. As model cells, we used sheep erythrocytes, which are sensitive to the pore-forming (haemolytic) activity of RtxA [21] and are commonly used as model cells for testing the pore-forming activity of RTX toxins [17].

First, it was necessary to identify an osmoprotectant that could block the membrane pores formed by RtxA and thus prevent osmotic lysis of erythrocytes, even at the relatively high amounts of the cell-bound RtxA molecules required for LC-MS/MS analysis. As osmoprotectants, we tested maltose, saccharose, and PEG molecules with average molecular weights of 400, 1000, 1500, 2000 and 3000 g/mol. As shown in Fig. 2A, the lysis of erythrocytes (5 × 10^8 cells/ml) by RtxA (1 μg/ml) was only partially reduced by maltose, saccharose and PEG 400, but completely blocked by PEG compounds with average molecular weights of 1000 g/mol and higher. Subsequent experiments with the PEG osmoprotectants showed that PEG 1500 and PEG 2000 completely blocked the lysis of erythrocytes incubated with RtxA even at concentrations of up to 30 μg/ml (Fig. 2B). When the PEG-supplemented buffer was exchanged for a buffer without PEG, erythrocytes were immediately lysed, indicating correct insertion of the RtxA molecules into the membrane and formation of functional toxin pores in the presence of the PEG molecules.

In the next step, the purified His-tagged RtxA toxin (30 μg/ml) was incubated with erythrocytes (5 × 10^8 cells/ml) in the presence of PEG 1500 and extracellular parts of the cell-bound RtxA molecules were labelled with the membrane-impermeable, lysine-reactive sulfo-NHS-LC-biotin (sulfo-biotin) reagent. After quenching of the unreacted reagent, the erythrocytes were washed with alkaline carbonate to remove loosely bound RtxA molecules and then transferred to a buffer without PEG 1500, resulting in immediate lysis of the erythrocytes. The labelled RtxA molecules were then purified from the solubilised membranes

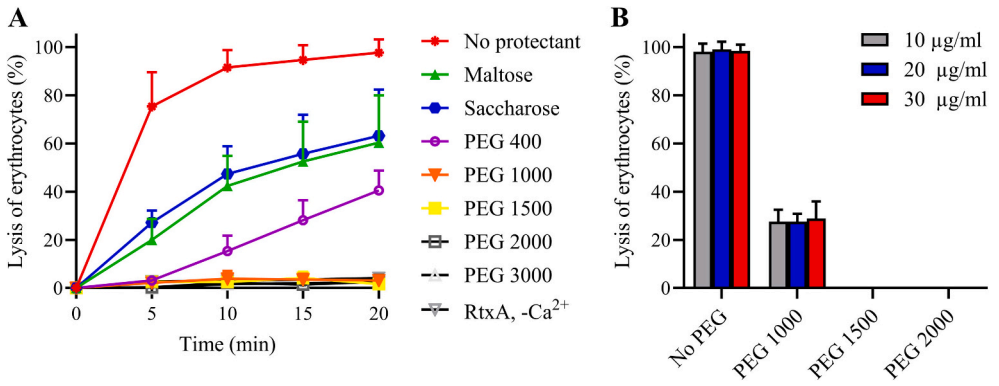

Fig. 2. PEG compounds with average molecular weights of 1500 g/mol and higher block the lysis of RtxA-treated erythrocytes. **(A)** Sheep erythrocytes (5×10^8 cells/ml) were incubated with purified RtxA (1 µg/ml) in the presence of various osmoprotectants at 37 °C. Erythrocytes incubated with RtxA in the absence of calcium ions served as a negative control. Lysis of erythrocytes was measured at various time points as the amount of released haemoglobin by photometric determination. Complete lysis of erythrocytes was reported as 100 %. Each point represents the mean value with SD of three independent determinations performed in duplicate. RtxA lysed erythrocytes with significantly lower efficiency in the presence of the osmoprotectants than in their absence ($p < 0.0001$ at all tested time points > 0). **(B)** Erythrocytes (5×10^8 cells/ml) were incubated with high concentrations of purified RtxA (10, 20 and 30 µg/ml) in the presence of PEG 1000, PEG 1500, and PEG 2000 for 60 min at 37 °C. Lysis of erythrocytes was measured as described in panel (A). Each bar represents the mean value with SD of three independent determinations performed in duplicate. RtxA lysed erythrocytes with significantly lower efficiency in the presence of the PEG osmoprotectants than in their absence (****, $p < 0.0001$).

using Ni-NTA agarose beads, digested with trypsin, and the generated peptides were analysed by LC-MS/MS.

As summarised in Fig. 3A, all 17 lysine residues in the N-terminus of RtxA (residues 1 to 130) were extracellularly labelled with sulfo-biotin, indicating that this part of the toxin remains completely outside the cell. As further shown in Fig. 3A, the pore-forming domain (residues 131 to

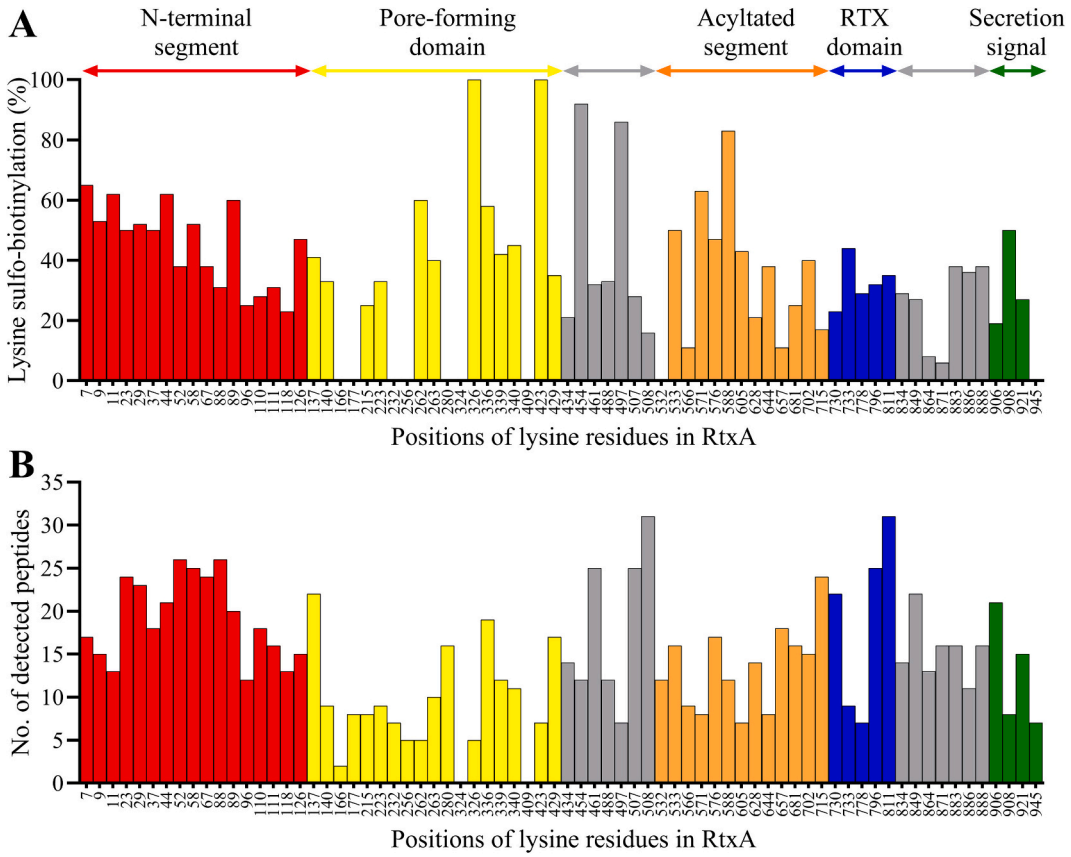

Fig. 3. Most of the cell-bound RtxA molecule is located extracellularly. **(A)** Purified His-tagged RtxA (30 µg/ml) was incubated with erythrocytes (5×10^8 cells/ml) in the presence of PEG 1500 for 15 min at 37 °C. After washing, the cell-bound RtxA molecules were labelled with the membrane-impermeable lysine-reactive sulfo-biotin reagent for 45 min. After quenching of the unreacted reagent, the erythrocytes were washed with alkaline carbonate to remove loosely bound RtxA molecules and then lysed by transfer to a buffer without PEG 1500. The labelled RtxA molecules were purified from the solubilised membranes using Ni-NTA agarose beads, digested with trypsin and the resulting peptides were analysed by LC-MS/MS. The percentage of sulfo-biotinylation at each lysine residue **(A)** was calculated as the ratio of the number of peptides sulfo-biotinylated at that lysine residue to the total number of corresponding peptides **(B)** detected in nine independent experiments. Peptides containing residues K324 and K409 were not identified by LC-MS/MS in any of the experiments. The acylated residues K558 and K689 are not shown.

430) of RtxA included 12 out of 19 lysine residues, namely K137, K140, K215, K223, K262, K263, K326, K336, K339, K340, K423 and K429, which were extracellularly labelled with sulfo-biotin. The residues K166, K177, K232, K256 and K280 remained unlabelled, indicating that these residues are located intracellularly or tightly associated with the cytoplasmic membrane, making them inaccessible to sulfo-biotinylation (Fig. 3A). The peptides with the remaining two lysine residues (K324 and K409) were not identified at all (Fig. 3B). These results indicate that the sulfo-biotinylated and sulfo-unbiotinylated lysine residues may delineate the extramembranous loops connecting the predicted transmembrane α-helices of the pore-forming domain of RtxA. The region comprising residues 431 to 510 contains 7 lysine residues, all of which were sulfo-biotinylated (Fig. 3A). Similarly, most of the 13 lysine residues in the acylated segment (residues 511 to 725) were labelled with sulfo-biotin, except for the K532 residue, which is adjacent to the sulfo-biotinylated K533 residue (Fig. 3A). The calcium-binding RTX domain (residues 726 to 815) of RtxA contains 5 lysine residues, all of which were sulfo-biotinylated (Fig. 3A). Finally, almost all 11 lysine residues, except for the last one (K945), located in the C-terminus of RtxA (residues 816 to 956), were extracellularly labelled (Fig. 3A). All these results demonstrate that 63 out of 72 lysine residues (87.5 %), evenly distributed along the entire RtxA molecule, were extracellularly labelled with sulfo-biotin, indicating that most of the toxin molecule is located outside the cell.

3.2. Five of the predicted transmembrane α-helices in the pore-forming domain of RtxA are irreversibly embedded in the membrane

Various algorithms were used to predict the transmembrane α-helices in the pore-forming domain of RtxA (Table 1). Almost all algorithms identified three transmembrane α-helices in the C-terminal region of the pore-forming domain, spanning residues 291 to 420 (Table 1). Some of the algorithms also predicted the presence of one to four additional transmembrane α-helices in the N-terminal part of the pore-forming domain, between residues 130 to 295 (Table 1).

To experimentally determine which of the seven predicted transmembrane α-helices of RtxA are irreversibly embedded in the membrane, purified RtxA (30 μg/ml) was incubated with erythrocytes (5×10^8 cells/ml) in the presence of PEG 1500. The unbound toxin molecules were then washed out and the erythrocytes were transferred to a buffer without PEG 1500 but containing trypsin (10 μg/ml). This led to immediate lysis of the erythrocytes and cleavage of the extramembranous segments of RtxA. The RtxA digests loosely associated with the membrane were removed with alkaline carbonate and the toxin segments irreversibly inserted into the membrane were isolated, digested and analysed by LC-MS/MS. As shown in Fig. 4A and Fig. S1A, most of the peptides isolated from the erythrocyte membranes covered the RtxA sequence spanning residues ~264–406, including the last four predicted transmembrane α-helices (Table 1). Within this region, either no or only low peptide coverage was observed in a segment comprising residues ~325–363 (Fig. 4A), indicating that this segment may form a long extramembranous loop connecting α-helix$_{297–319}$ and α-helix$_{361–380}$ (Table 1). Since the residues K326, K336, K339 and K340 within this loop were sulfo-biotinylated (Fig. 3A), the loop is localised extracellularly. Some of the membrane-isolated peptides also covered the third predicted transmembrane α-helix$_{235–254}$ (Table 1) but not the adjacent segment delineated by residues K256 and K263 (Fig. 4A). This indicates that the segment may form an extramembranous loop connecting α-helix$_{235–254}$ and α-helix$_{264–289}$. The residues K262 and K263 within this loop were labelled with sulfo-biotin (Fig. 3A), which indicates its extracellular localization. Importantly, no peptides, or only trace amounts of peptides, were detected in the N- and C-terminal parts of RtxA, encompassing residues M1 to ~K232 and ~K409 to V956, respectively (Fig. S1A). This observation is consistent with the data presented above, which show that most of the lysine residues in these two regions of the membrane-bound RtxA were sulfo-biotinylated (Fig. 3A) and thus located outside the cell.

Similar results were obtained when the experiment was performed on liposomes, which were previously shown to be an excellent model for binding studies of RtxA [21]. As shown in Fig. 4B and Fig. S1B, most of the peptides isolated from the liposome membranes covered a sequence encompassing the last five predicted transmembrane α-helices (Table 1), while no peptides, or only trace amounts of peptides, were detected in the N- and C-terminal parts of RtxA.

Taken together, five out of the seven transmembrane α-helices predicted in the pore-forming domain of RtxA (Table 1) were experimentally shown to be irreversibly embedded in the membranes of both erythrocytes and liposomes, indicating that at least some of these helices could be part of an ion-conducting membrane pore.

3.3. Structure-function analysis of RtxA

Based on the predictions and experimental results, we constructed, produced and purified a set of deletion mutants of His-tagged RtxA

Table 1
Transmembrane α-helices (TMHs) of RtxA predicted by different algorithms.

Algorithm	TMH-1	TMH-2	TMH-3	TMH-4	TMH-5	TMH-6	TMH-7	Reference
	(Amino acid residues in RtxA)							
Membrain 2.0	130–157	173–200	231–253	258–293	296–321	347–420		[53]
MEMSAT-SMV				274–289	302–317	369–399		[54]
OCTOPUS			235–255		301–321	363–383	385–405	[55]
Philius					292–318	371–405		[56]
POLYPHOBIUS			235–254		291–305, 307–321	366–382	384–405	[57]
PRO			233–253	274–294	299–319	362–382	385–405	[58]
PRODIV	141–161		233–253	274–294	299–319	362–382	385–405	[58]
RHYTHM				276–295	300–319	363–382	387–405	[59]
SPLIT Server			236–252		295–320	362–382	386–406	[60]
SPOCTOPUS					298–318	362–382	384–404	[60]
SCAMPI-msa			235–255		301–321	363–383	385–405	[61]
SCAMPI-seq	144–164		235–255		299–319		385–405	[61]
TMSEG					299–313		384–402	[62]
TMPred	143–159		235–254		301–319		382–405	[63]
TOPCONS	144–164		233–253	274–294	299–319	362–382	385–405	[64]
Prediction frequency[a]	33 %	7 %	67 %	40 %	100 %	80 %	100 %	
Deletions[b]	143–159	177–201	235–254	264–289	297–319	361–380	386–406	

[a] The percentage of the algorithms that predicted the given α-helix to be transmembrane.
[b] Seven RtxA variants lacking the predicted α-helix$_{143–159}$, α-helix$_{177–201}$, α-helix$_{235–254}$, α-helix$_{264–289}$, α-helix$_{297–319}$, α-helix$_{361–380}$ or α-helix$_{386–406}$ were constructed, produced, purified and characterised.

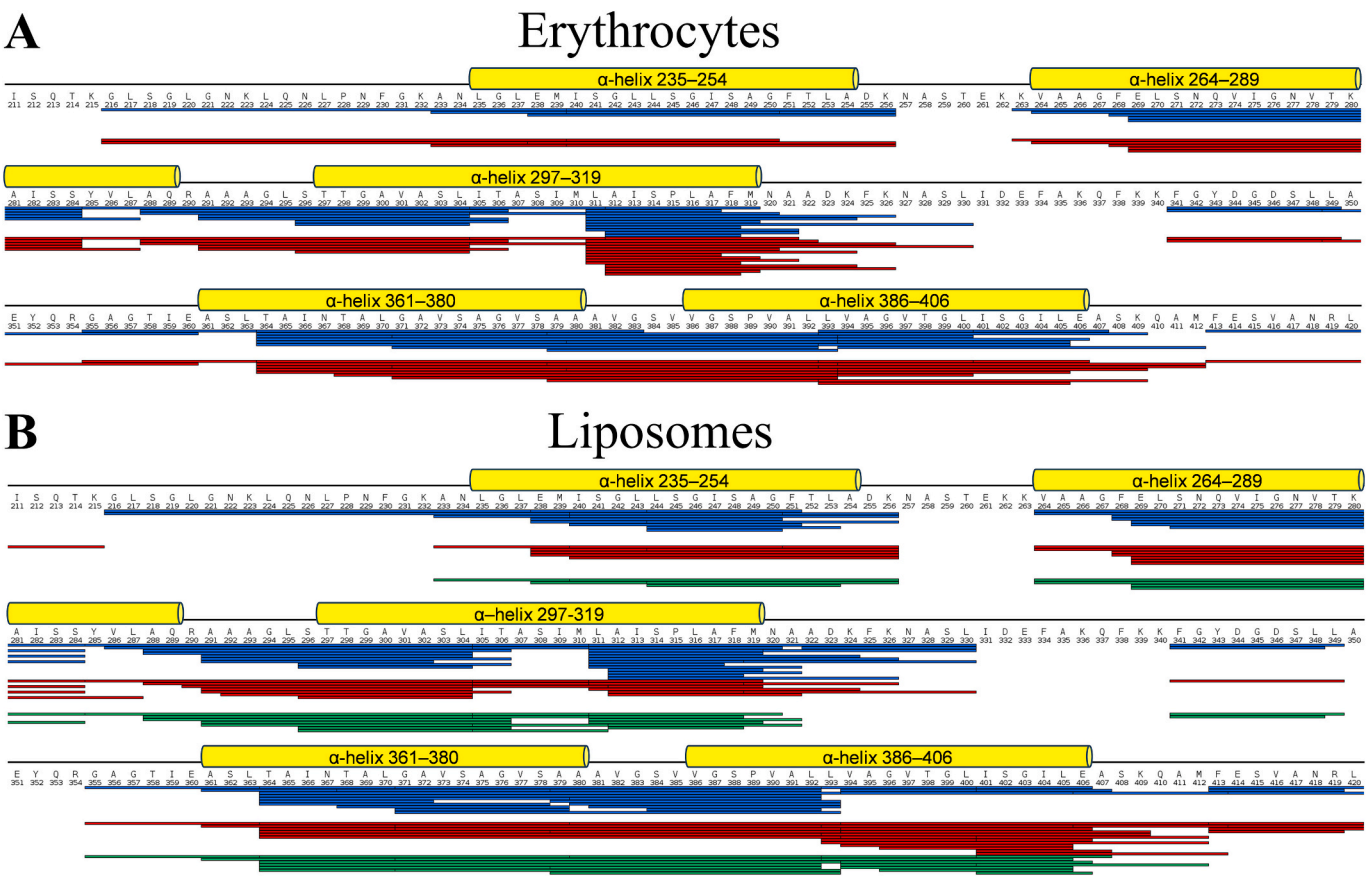

Fig. 4. Five of the seven predicted transmembrane α-helices of RtxA are irreversibly inserted into the membrane of erythrocytes and liposomes. Purified RtxA was incubated with erythrocytes **(A)** or cholesterol-containing liposomes **(B)**, as described in Materials and methods. After washing, both erythrocytes and liposomes were resuspended in a buffer containing mass spectrometry grade trypsin, which cleaved the extramembranous segments of RtxA. Toxin segments loosely associated with the membrane were removed with alkaline carbonate, while membrane-inserted segments were isolated, digested and analysed by LC-MS/MS. The peptide coverage of the RtxA sequence from two (blue and red) (A) or three (blue, red and green) independent experiments (B) is shown. The five predicted α-helices (Table 1) are shown as yellow cylinders above the RtxA sequence.

(Fig. 1C) and used them for structure-function analysis of the toxin.

First, we utilised CD spectroscopy to analyse the secondary structure of the RtxA molecule, which should mainly consist of α-helices, β-sheets and turns, as indicated by the AlphaFold model (Fig. 1A). Additionally, we investigated whether RtxA undergoes folding upon binding of calcium ions to the conserved nonapeptide repeat sequences within the RXT domain, as has been demonstrated for other RTX toxins [16–18]. As shown in Fig. 5A, when the urea-denatured RtxA toxin was refolded in the absence of calcium ions, the CD spectrum indicated a protein molecule with a mix of α-helices and β-sheets, alongside some unstructured regions. Upon the addition of a buffer containing a physiological concentration of calcium ions (2 mM), the RtxA molecule underwent significant conformational changes. This was evidenced by an increase in the negative intensity of the peak at ~220 nm and an increase in the signal at 200 nm, indicating a reduction in the unfolded regions and an increase in the content of β-sheets due to calcium-dependent folding (Fig. 5A). The presence of a shoulder as a remnant of the peak at 208 nm further confirmed that the final folded structure of RtxA contains a

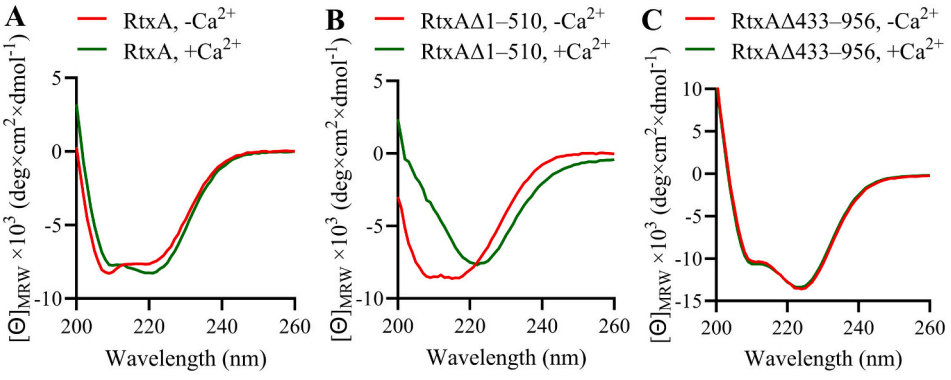

Fig. 5. The RtxA molecule undergoes significant conformational changes upon the binding of calcium ions. Urea-unfolded intact RtxA **(A)** and its deletion variants RtxAΔ1–510 **(B)** and RtxAΔ433–956 **(C)** were refolded in a buffer without or with calcium ions and CD spectra of the proteins were acquired in the far ultraviolet range from 200 to 260 nm. Each protein was measured in two independent experiments, with three accumulations per experiment.

mixture of α-helices and β-sheets (Fig. 5A). The calcium-dependent folding was even more pronounced in the RtxAΔ1–510 variant, which lacks the N-terminal half of the toxin (Fig. 5B). In contrast, the truncated RtxAΔ433–956 protein, comprising the N-terminal segment and the pore-forming domain, did not undergo calcium-dependent conformational changes, as evidenced by the nearly identical spectra of the protein in a buffer without or with calcium ions (Fig. 5C). The CD spectra indicate a mixture of α-helices and β-sheet structures, with α-helices being the predominant structure. The negative bands around 222 nm and 208 nm, along with a positive band near 200 nm, are characteristic of an α-helix-rich structure. However, the typical spectra of proteins that are exclusively or predominantly α-helical show similar ellipticity values at 208 and 222 nm, whereas the CD spectrum of the folded RtxAΔ433–956 protein shows a weaker negative band at 208 compared to that at 222 nm (Fig. 5C). This difference indicates the presence of some β-sheets within the protein, further supporting the AlphaFold model shown in Fig. 1A.

Next, we analysed the capacity of the RtxA deletion mutants to bind and lyse erythrocytes. To analyse binding, erythrocytes (1×10^7 cells/ml) were incubated with varying concentrations of the purified RtxA mutants (0–38 nM). Unbound RtxA molecules were removed with alkaline carbonate and the cell-bound toxin molecules were stained with a fluorescently labelled anti-His antibody and detected by flow cytometry. All procedures were carried out in buffers supplemented with PEG 1500 to prevent erythrocyte lysis. As shown in Fig. 6A, all RtxA mutants with deletions in the N-terminal half of the molecule (RtxAΔ1–130, RtxAΔ1–231, RtxAΔ1–255, RtxAΔ1–430 and RtxAΔ1–510) but with an intact C-terminal half (residues 511–956) bound erythrocytes with similar efficiency as intact RtxA. As the mutants could not be removed with alkaline carbonate, the C-terminal half of RtxA is most likely sufficient for both the interaction of the toxin with glycosylated cell surface structures [23,24] and the irreversible insertion of the toxin into the membrane. This insertion primarily occurred via the acyl chains covalently bound to the residues K558 and K689 [21,22], rather than through the transmembrane α-helices of the pore-forming domain, which were completely deleted in the RtxAΔ1–430 and RtxAΔ1–510 mutants. Furthermore, nonacylated proRtxA did not insert into the membrane at all (Fig. 6A). Correspondingly, only trace amounts of the RtxAΔ433–956 mutant bound to the surface of erythrocytes (Fig. 6A), confirming that the C-terminal half of the toxin is essential for its full binding and insertion into the membrane. Similarly, only residual binding was observed with the RtxAΔ624–956 mutant (Fig. 6A), which consists of the N-terminal half of the toxin and the first acylation site, where the K558 residue is only partially acylated [21,22]. Interestingly, cell-binding of the RtxAΔ725–956 mutant, which in addition contains the second acylation site with the fully acylated K689 residue [21,22], was 40 % (calculated from binding values at all concentrations) of that of intact RtxA (Fig. 6A). This indicates that the acyl chains covalently linked to the K689 residue enable at least partial, irreversible binding of the RtxAΔ725–956 mutant to the cell membrane.

To analyse haemolytic activity, erythrocytes (5×10^8 cells/ml) were incubated with the RtxA deletion mutants at a final concentration of 3.8 nM for various time points (0–30 min). As shown in Fig. 6B, the RtxAΔ1–130 mutant lysed the cells with an approximately 4-fold lower efficiency than the intact toxin (calculated from haemolytic activity values at 5, 10 and 15 min), indicating that the first 130 extracellular residues significantly modulate the pore-forming activity of the toxin. The RtxA mutants with deletions of the first two (RtxAΔ1–231), three (RtxAΔ1–255) or all (RtxΔ1–430 and RtxΔ1–510) predicted transmembrane α-helices (Fig. 1C and Table 1) showed residual or no haemolytic activity (Fig. 6B). When the concentration of these mutants was increased to 19 nM, the RtxAΔ1–231 mutant, but not the RtxAΔ1–255, RtxΔ1–430 and RtxΔ1–510 mutants, exhibited low but significantly higher haemolytic activity than proRtxA (Fig. S2). This indicates that the first two predicted transmembrane α-helices, α-helix$_{143–159}$ and α-helix$_{177–201}$ (Table 1), which, however, were not experimentally confirmed to be embedded in the membrane (Fig. S1), are likely not part of the ion-conducting membrane pore but significantly influence its formation. Additionally, the RtxAΔ441–484 mutant, which has a partial deletion in the segment linking the pore-forming domain and the acylated segment, bound to erythrocytes similarly to the intact RtxA (Fig. 6A), but completely lost its haemolytic activity (Fig. 6B). This

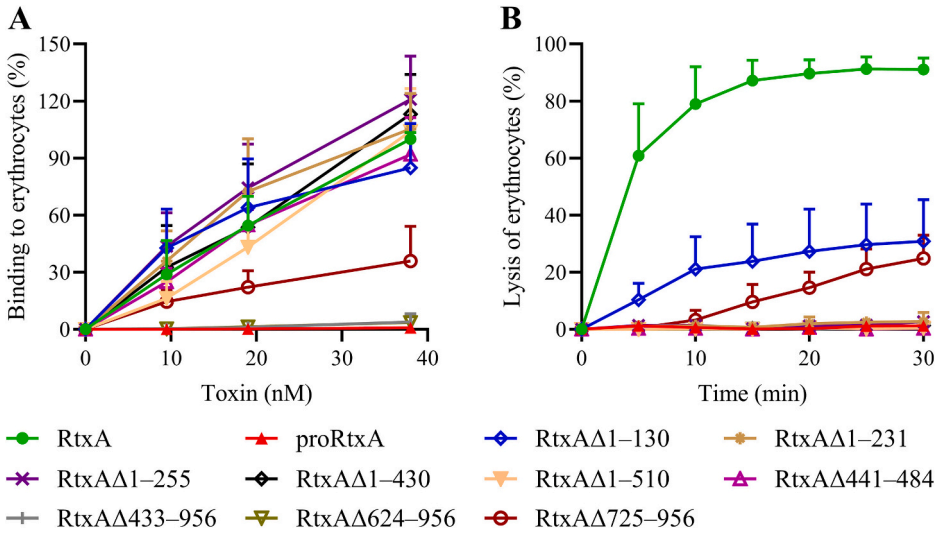

Fig. 6. All parts of RtxA are required for its full lytic activity. **(A)** Sheep erythrocytes (5×10^8 cells/ml) were incubated with various concentrations of the RtxA variants (0 to 38 nM) for 15 min at 22 °C. After washing, the cell-bound RtxA molecules were stained with a fluorescently labelled antibody and detected by flow cytometry. Binding data were derived from the MFI values and expressed as the percentage of intact RtxA binding to erythrocytes at a concentration of 38 nM (taken as 100 %). Each point represents the mean value with SD of at least six independent determinations performed in duplicate. The binding of proRtxA ($p < 0.0001$), RtxAΔ433–956 ($p < 0.0001$), RtxAΔ624–956 ($p < 0.0001$) and RtxAΔ725–956 ($p < 0.05$–$p < 0.0001$) to erythrocytes was significantly lower than that of intact RtxA at all measured concentrations. **(B)** Erythrocytes (5×10^8 cells/ml) were incubated with purified RtxA variants (3.8 nM) and cell lysis was measured at various time points as the amount of released haemoglobin by photometric determination. Complete lysis of erythrocytes was reported as 100 %. Each point represents the mean value with SD of three independent determinations performed in duplicate. All RtxA mutants lysed erythrocytes with significantly lower efficiency than intact RtxA ($p < 0.0001$ at all tested time points > 0).

indicates that the linking segment of the bound RtxA is crucial for the correct positioning of the pore-forming domain relative to the membrane and/or its subsequent correct insertion. Finally, the RtxAΔ725–956 mutant, despite its lower binding capacity (Fig. 6A), still exhibited detectable haemolytic activity (Fig. 6B), indicating that the RtxA molecule lacking the C-terminal RTX domain and secretion signal can, at least partially, form functional membrane pores. All these results indicate that the precise interplay of all regions of RtxA is essential for its full pore-forming activity.

3.4. *All five α-helices in the pore-forming domain of RtxA are crucial for its pore-forming activity*

To analyse which of the five predicted and experimentally confirmed membrane-embedded α-helices might be part of the ion-conducting membrane pore of RtxA, we constructed five toxin variants, each lacking one of the following α-helices: α-helix$_{235–254}$, α-helix$_{264–289}$, α-helix$_{297–319}$, α-helix$_{361–380}$ or α-helix$_{386–406}$ (Table 1). Additionally, we constructed RtxA variants with deletions of the α-helix$_{143–159}$ or α-helix$_{177–201}$, which were predicted by some of the algorithms (Table 1), but not experimentally confirmed (Fig. S1), to be transmembrane. As shown in Fig. 7A, most of the RtxA mutants bound to erythrocytes with a similar capacity as intact RtxA. Only the RtxAΔ386–406 mutant exhibited a reduced binding capacity compared to intact RtxA (on average by 48 %) (Fig. 7A), indicating that the deletion of the α-helix$_{386–406}$ may induce conformational changes in the toxin molecule that negatively affect its binding to the cell surface and/or irreversible insertion into the membrane.

As shown in Fig. 7B, both RtxAΔ143–159 and RtxAΔ177–201 exhibited haemolytic activity, although significantly reduced compared to intact RtxA (on average by 75 % and 93 %, respectively), but still significantly higher compared to proRtxA. This further supports our observations indicating that the α-helix$_{143–159}$ and α-helix$_{177–201}$ are not part of the ion-conducting membrane pore but play an important role in its formation. Among the RtxA mutants lacking the experimentally confirmed membrane-associated α-helices (Fig. 4), only RtxAΔ297–319 exhibited residual haemolytic activity, but this was not significantly higher than that of proRtxA (Fig. 7B). The other four RtxA mutants (RtxAΔ235–254, RtxAΔ264–289, RtxAΔ361–380 and RtxAΔ386–406) were unable to lyse erythrocytes at all (Fig. 7B).

To corroborate our observations on erythrocytes, we analysed the RtxA mutants using artificial lipid bilayers composed of 3 % asolectin. Consistent with the residual haemolytic activity observed on erythrocytes, the RtxAΔ297–319 mutant also exhibited very low overall membrane activity on lipid bilayers when compared to intact RtxA (Fig. 8A). In addition, the few single pores formed by RtxAΔ297–319 were not well-defined and exhibited substantially lower currents than the pores formed by intact RtxA (Fig. 8B and Fig. S3). This indicates that the α-helix$_{297–319}$ directly affects the toxin pore and could serve as its structural element. The RtxA mutants lacking the α-helix$_{235–254}$, α-helix$_{264–289}$, α-helix$_{361–380}$ or α-helix$_{386–406}$ were completely inactive on lipid bilayers (Fig. 8), as they were on erythrocytes (Fig. 7B), indicating that at least some of these α-helices could be integral parts of the ion-conducting pore.

Finally, we substituted single residues at the beginning, middle or end of each membrane-embedded α-helix with a helix-breaking proline residue. As shown in Fig. S4, the RtxA mutants with point substitutions within the α-helix$_{386–406}$ exhibited an almost complete loss of haemolytic activity on erythrocytes. Most of the point substitutions introduced into the other four α-helices reduced the haemolytic activity of the mutants by 13–87 % of that of intact RtxA. These results further confirm that all identified membrane-associated α-helices are crucial for the lytic activity of RtxA, with the α-helix$_{386–406}$ being the most critical. These findings also indicate that these α-helices, particularly the α-helix$_{386–406}$, may serve as structural elements of the ion-conducting membrane pore of RtxA.

4. Discussion

Dozens of studies have demonstrated that RTX toxins bind to various eukaryotic cells, insert into the membrane and cause cell lysis through the formation of membrane pores [16–18]. However, despite extensive research, the precise membrane topology of RTX toxins remains unknown, largely due to experimental challenges such as the tendency of RTX toxins to aggregate in solution, the limited number of toxin molecules inserted into the cell membrane and the rapid lysis of affected cells. To address these issues, we developed a novel approach that involves incorporating high amounts of the RtxA toxin into the cell membrane in

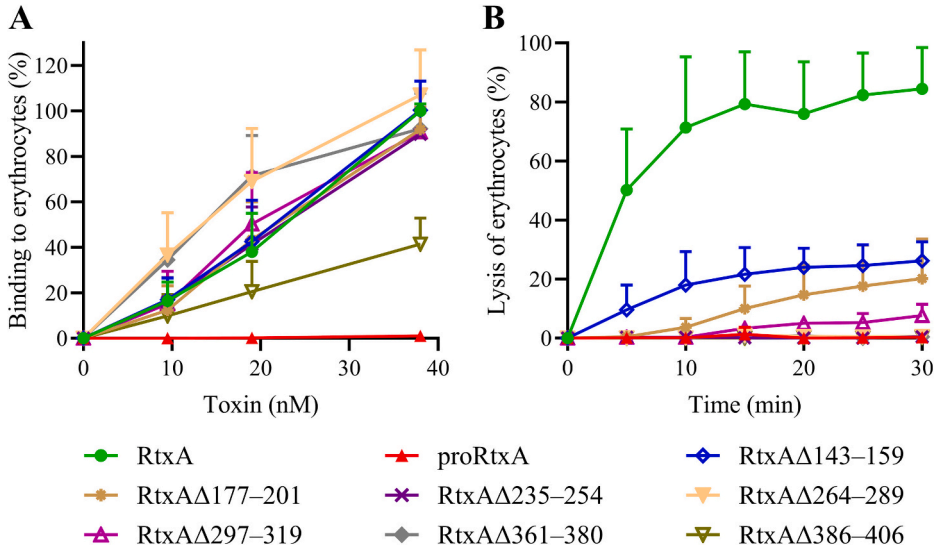

Fig. 7. Deletion of the α-helix$_{235–254}$, α-helix$_{264–289}$, α-helix$_{361–380}$ or α-helix$_{386–406}$ leads to a complete loss of lytic activity of RtxA. The binding **(A)** and haemolytic **(B)** activities of the RtxA variants were measured as described in the legend to Fig. 6. **(A)** Each point represents the mean value with SD of at least four independent determinations performed in duplicate. The binding of proRtxA and RtxAΔ386–406 to erythrocytes was significantly lower than that of intact RtxA ($p < 0.01$–$p < 0.0001$) at all measured concentrations for proRtxA and at concentrations >10 nM for RtxAΔ386–406. **(B)** Each point represents the mean value with SD of three independent determinations performed in duplicate. All RtxA mutants lysed erythrocytes with significantly lower efficiency than intact RtxA ($p < 0.0001$ at all tested time points > 0).

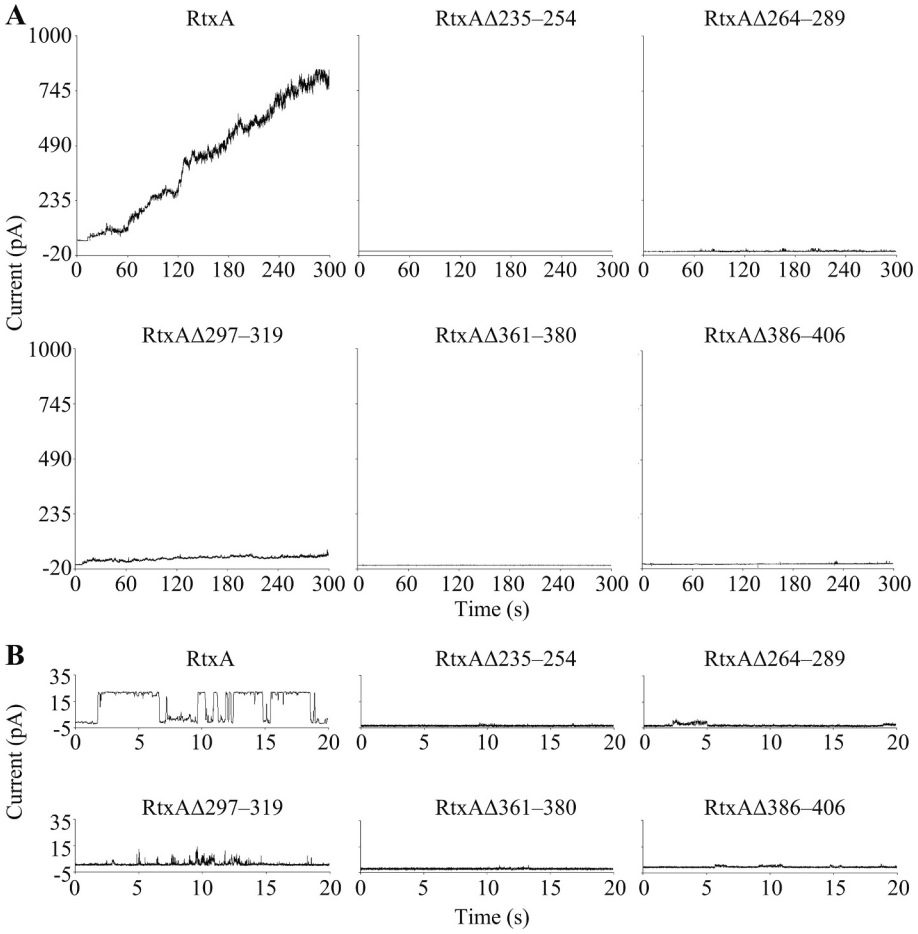

Fig. 8. RtxA variants lacking the α-helix$_{235–254}$, α-helix$_{264–289}$, α-helix$_{361–380}$ or α-helix$_{386–406}$ are unable to form ion-conducting membrane pores. **(A)** Overall membrane activities of the RtxA variants on asolectin/decane:butanol (9:1) membranes in the presence of 250 pM purified proteins. The aqueous phase contained 150 mM KCl, 10 mM Tris-HCl (pH 7.4), 2 mM $CaCl_2$. The temperature was maintained at 22 °C; a voltage of 50 mV was applied, and the recordings were filtered at 10 Hz. **(B)** Single-pore recordings of asolectin membranes in the presence of 10 pM RtxA variants under otherwise identical conditions as in (A).

the presence of an osmoprotectant, followed by either labelling of cell-bound toxin molecules with a sulfo-biotinylation reagent or cleaving them with trypsin. These strategies enabled us to identify the extracellular parts as well as membrane-inserted segments of RtxA by highly sensitive MS. In combination with other biophysical, bioinformatic, molecular biological and biochemical methods, this approach allowed us to propose a membrane topology model of RtxA, as depicted in Fig. 9.

In this model, the N-terminal segment of RtxA, which includes the first 231 residues, is located extracellularly (Fig. 9A), as it contains 21 of the 23 lysine residues labelled with the membrane-impermeable sulfo-biotin reagent. The remaining two unlabelled residues, K166 and K177, are located between the α-helix$_{143–159}$ and α-helix$_{177–201}$, both of which some algorithms predicted as transmembrane (Table 1). However, our experiments identifying the transmembrane segments of RtxA in the membranes of erythrocytes and liposomes indicate that these two α-helices are located extracellularly rather than within the membrane. Therefore, it seems more likely that the segment containing the unlabelled residues K166 and K177 is oriented from the extracellular side towards the membrane, making these two lysine residues inaccessible for the sulfo-biotin reagent. Functional analysis of RtxA mutants with the deletions Δ1–130 and Δ1–231 showed that while the N-terminal segment does not participate in the binding of RtxA, it significantly reduces the haemolytic activity of the toxin. These findings indicate that the N-terminal segment modulates the pore-forming activity of RtxA but is not part of the ion-conducting membrane pore. Similarly, it was previously hypothesised that the N-terminal segment of α-haemolysin (HlyA), an RTX toxin secreted by *E. coli*, is not part of the membrane pore but may function as its regulator [36]. This hypothesis was based on the observation that HlyA mutants with N-terminal deletions Δ10–19 and Δ9–37 exhibited haemolytic activity that was 1.5- and 2.5-fold higher, respectively, than that of intact HlyA [36]. Additionally, the haemolytic activity of the RTX adenylate cyclase toxin (CyaA) of *Bordetella pertussis* was significantly enhanced upon the deletion of its N-terminal part (Δ6–489), which includes the enzymatic adenylate cyclase (AC) domain and an adjacent membrane-interacting segment preceding the pore-forming domain of the toxin [37,38]. Furthermore, substitutions of negatively charged residues in the segment linking the AC domain to the pore-forming domain of CyaA also markedly increased haemolytic activity of the toxin [39]. The results from RtxA, HlyA and CyaA thus show that the N-terminal segment can modulate the lytic activity of these toxins in both directions, depending on the type of the introduced deletions and substitutions.

The N-terminal segment of RtxA is followed by five α-helices (Fig. 9A). Of these, two (α-helix$_{297–319}$ and α-helix$_{386–406}$) were predicted to be transmembrane by all algorithms, while the remaining three (α-helix$_{235–254}$, α-helix$_{264–289}$ and α-helix$_{361–380}$) were predicted to be transmembrane by only some of them (Table 1). Our experiments demonstrated that all these five predicted α-helices in membrane-bound RtxA were protected from trypsin cleavage, indicating that they are inserted in the membrane.

The membrane-inserted α-helix$_{264–289}$ and α-helix$_{297–319}$ form a first pair of back-to-back α-helices connected by a very short loop of 7 amino

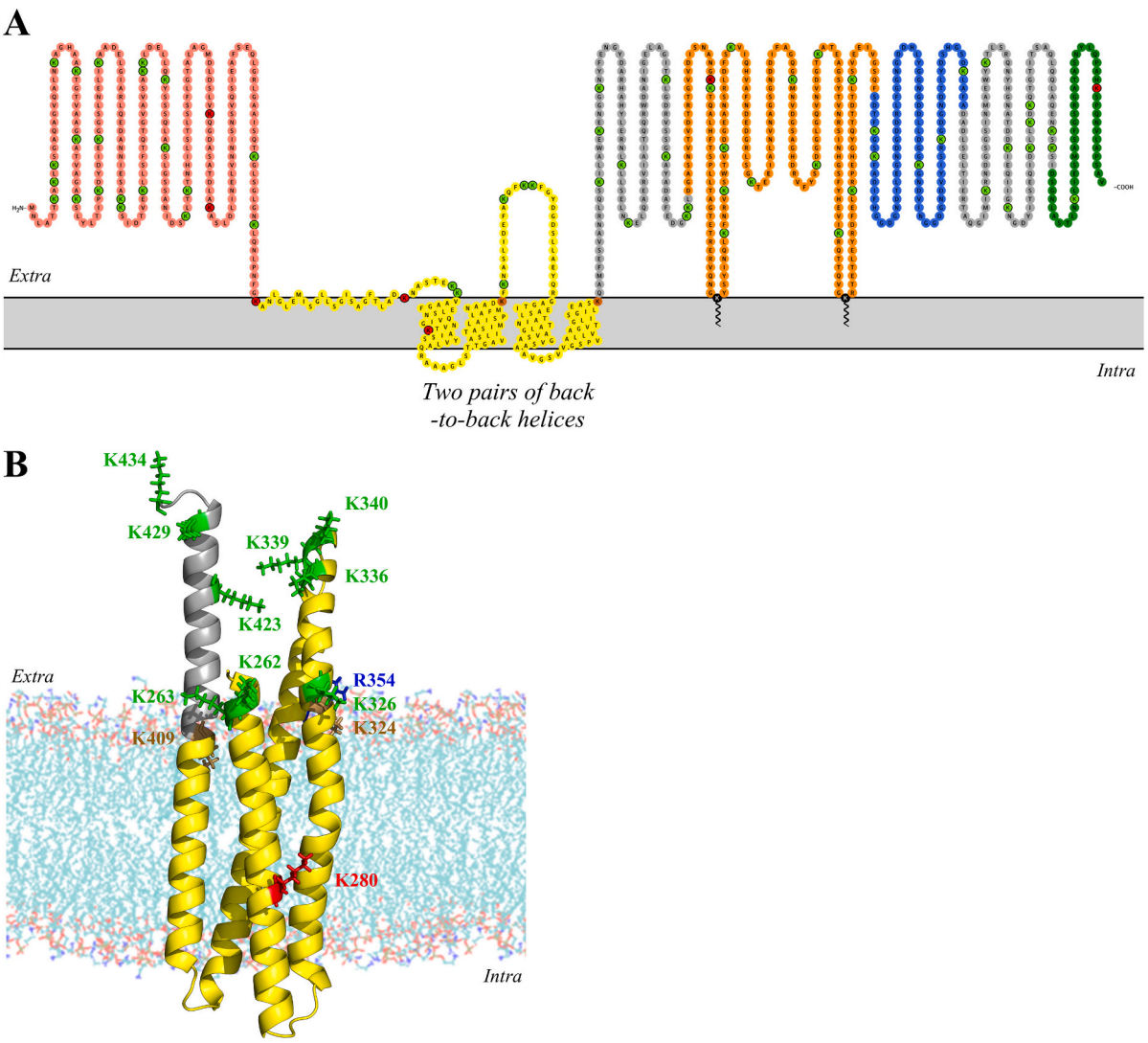

Fig. 9. Model of the membrane topology of RtxA. **(A)** Graphical representation of the membrane topology of RtxA based on experimental data and generated with the Protter Server [52]. Lysine residues labelled with sulfo-biotin are highlighted in green, while unlabelled lysine residues are shown in red. Peptides containing residues K324 and K409 (coloured in brown) were not identified by LC-MS/MS. The two pairs of back-to-back helices span the membrane bilayer. The acyl chains covalently linked to the conserved residues K558 and K689 anchor the toxin in the membrane. **(B)** Detail of the two pairs of back-to-back α-helices of RtxA extracted from the AlphaFold structure of the toxin and fitted into the membrane. The colour coding of the lysine residues (shown as sticks) is described in (A). The positively charged residues K262, K263, K324, K326, R354 (coloured in blue) and K409 located near the membrane might serve as membrane interfacial anchors in the proposed structure of RtxA.

acid residues (Fig. 9A and B). While the RtxAΔ297–319 mutant, which lacks the α-helix$_{297–319}$, exhibited residual haemolytic activity on erythrocytes and correspondingly low overall membrane activity on planar lipid membranes, the RtxAΔ264–289 mutant, which lacks the α-helix$_{264–289}$, showed no lytic activity on erythrocytes and no pore-forming activity on planar lipid membranes. However, the residual haemolytic activity of RtxAΔ297–319 was not significantly higher than that of proRtxA and the few single pores formed by this mutant in planar lipid membranes were not well-defined and exhibited a significantly lower current than the pores formed by intact RtxA. This indicates that both the α-helix$_{264–289}$ and the α-helix$_{297–319}$ could be part of the ion-conducting membrane pore formed by RtxA. Therefore, we propose that these two hydrophobic α-helices could span the membrane bilayer, with the short loop connecting them inside the cell cytosol. The positively charged lysine residues K262 and K263 at the N-terminus of the α-helix$_{264–289}$ could anchor this helix to the extracellular side of the membrane bilayer, similarly to how the lysine residues K324 and K326 could anchor the α-helix$_{297–319}$ (Fig. 9A and B). This is supported by our data showing that the lysine residues K262, K263 and K326 were labelled extracellularly with the membrane-impermeable, lysine-reactive sulfo-biotin reagent (no peptide containing K324 was detected by LC-MS/MS). Indeed, it has been previously shown that lysine residues, along with arginine, tryptophane and tyrosine residues, are involved in anchoring membrane spanning α-helices to the membrane bilayer surface [40].

The membrane-inserted α-helix$_{361–380}$ and α-helix$_{386–416}$ form a second pair of back-to-back α-helices connected by a very short loop of 5 amino acid residues (Fig. 9A and B). The RtxAΔ361–380 and RtxAΔ386–406 mutants, which lacks these α-helices, exhibited no lytic activity on erythrocytes and correspondingly no overall membrane activity on planar lipid membranes. This indicates that the highly hydrophobic α-helix$_{361–380}$ and α-helix$_{386–406}$ could span the membrane bilayer and be part of the ion-conducting membrane pore. The short loop connecting both helices could be located intracellularly and the residues R354 and K409 could anchor these two α-helices to the extracellular side of the membrane bilayer (Fig. 9A and B). The two pairs of back-to-back

α-helices are connected by a long extracellular segment that links the α-helix$_{297–319}$ with the α-helix$_{361–380}$ and contains five lysine residues, four of which were labelled extracellularly with the membrane-impermeable sulfo-biotin (Fig. 9A and B). As shown in Fig. 9B, the transmembrane α-helix$_{297–319}$, α-helix$_{361–380}$ and α-helix$_{386–406}$ are predicted by the AlphaFold algorithm as extended α-helical structures that partially protrude from the membrane into the extracellular space.

In our previous study, we demonstrated that cholesterol facilitates the interaction of RtxA with artificial and cell membranes. Analysis of the primary sequence of RtxA revealed five putative cholesterol recognition/interaction amino acid consensus motifs located within or adjacent to the pore-forming domain, suggesting that at least some of them could mediate the interaction between RtxA and membrane cholesterol. The substitutions Y343F and Y352F in two of these five cholesterol-binding motifs indeed reduced the lytic capacity of the RtxA variants in erythrocytes to ~50 % of that of intact RtxA. Based on this result, we speculated that the two cholesterol-binding motifs, located between residues 340–354 of RtxA, might be involved in the interaction of the toxin with membrane cholesterol [21]. However, the data reported here indicate that these two cholesterol-binding motifs are localised in an extramembranous segment comprising residues ~325–363 (Fig. 9) and are not embedded in the membrane, where they could interact with membrane cholesterol. Therefore, other regions of RtxA are most likely responsible for interacting with membrane cholesterol, and the Y343F and Y352F substitutions introduced into the extramembranous segment might affect the spatial arrangement of adjacent transmembrane α-helical segments, leading to the partially reduced lytic activity of the toxin.

Finally, the last membrane-associated α-helix$_{235–254}$ of RtxA is localised between the long extracellular N-terminal part (residues 1–231) and the membrane-spanning α-helix$_{264–289}$ (Fig. 9A). The α-helix$_{235–254}$ is connected to the α-helix$_{264–289}$ by a very short extracellular loop containing two lysine residues (K262 and K263), which were labelled extracellularly with the membrane-impermeable sulfo-biotin reagent (Fig. 9A). Since the α-helix$_{235–254}$ is surrounded by extracellular segments and is too short to span the membrane bilayer from the extracellular to the intracellular side and back, it is more likely inserted only into the outer leaflet of the membrane (Fig. 9A). Furthermore, the RtxAΔ235–254 mutant, which lacks the α-helix$_{235–254}$, exhibited no lytic activity on erythrocytes and correspondingly showed no overall membrane activity on planar lipid membranes. All these results show that the α-helix$_{235–254}$ of RtxA plays a crucial role in pore formation.

Deletion mutagenesis of HlyA has previously demonstrated that the formation of membrane pores by the toxin depends on a hydrophobic region between residues 238–410 [36], which shares primary sequence homology with a corresponding hydrophobic region of RtxA (residues 233–405, 58 % identity, 78 % similarity). An HlyA mutant with a deletion of residues 238–259 (corresponding to the α-helix$_{235–254}$ of RtxA) retained residual activity on erythrocytes and exhibited increased conductance in planar lipid membranes compared to intact HlyA, but without forming well-defined pores. Two other HlyA mutants, with deletions of residues 299–327 (corresponding to the α-helix$_{297–319}$ of RtxA) and 366–410 (corresponding to the α-helix$_{361–380}$ and α-helix$_{386–406}$ of RtxA), showed completely abolished pore-forming activity. Furthermore, deletion of the single polar aspartate residue D243 within the hydrophobic segment 238–259 of HlyA significantly reduced the ability of the mutant toxin to form membrane pores, whereas the single substitutions D243E and D243N had minimal impact on pore formation [36]. Later experiments on membrane binding and insertion of HlyA were performed on liposomes containing a photoactivatable probe, which allowed labelling of the membrane-inserted segments of the toxin. The results demonstrated that the hydrophobic sequence comprising residues 177–411 is essential for toxin insertion [41]. Additionally, cysteine scanning mutagenesis of HlyA later identified an amphipathic α-helix between residues 272–298 that could line the membrane pore [42]. A double substitution G284P+I287P within this α-helix did not affect the binding of the mutant toxin to erythrocytes but completely abolished its haemolytic activity, highlighting the importance of G284 and I287 in the pore-forming activity of HlyA [42]. All these findings indicate that the hydrophobic segments, which are partially homologous between RtxA and HlyA, are crucial for the formation of ion-conducting membrane pores and their structural integrity is essential for the lytic activity of both RTX toxins.

In contrast to RtxA and HlyA, CyaA forms membrane pores with a significantly smaller diameter (0.6–0.8 nm for CyaA compared to 1.9 nm for RtxA, 1.4–3 nm for HlyA) [25,43,44]. The hydrophobic pore-forming domain of CyaA, predicted to be between residues ~500–700, is crucial not only for the formation of membrane pores but also for the translocation of the N-terminal enzymatic AC domain of the toxin across the membrane into the cell cytosol (cell-invasive AC activity) [45–48]. According to the algorithm of Eisenberg, the pore-forming domain of CyaA consists of five transmembrane α-helices, predicted to span residues 502–522, 529–549, 571–591, 607–627 and 678–698 [45,49]. While the first four α-helices are involved in both pore-forming and cell-invasive AC activity, the fifth α-helix is exclusively involved in the pore-forming activity of CyaA [45–48,50,51]. Nevertheless, there are no conclusive data showing which of the predicted α-helices of CyaA span the membrane and form an ion-conducting pore.

The C-terminal half of RtxA, located downstream of the α-helix$_{386–406}$, contains 39 lysine residues, 36 of which were labelled extracellularly with the membrane-impermeable sulfo-biotin reagent. Furthermore, when RtxA was inserted into the membranes of erythrocytes and liposomes and subsequently cleaved by trypsin, no peptides, or only trace amounts of peptides, were detected in the C-terminal half of the toxin by LC-MS/MS. This indicates that the entire C-terminal half of RtxA, including the acylated segment, RTX domain and C-terminal secretion signal, does not penetrate the cell membrane.

5. Conclusion

In this study, we have identified the extracellular regions of the membrane-bound RtxA molecule and the membrane-embedded segments crucial for the formation of ion-conducting pores. Based on our findings, we have designed a model of the membrane topology of RtxA. We believe that the new approaches developed in this study can also be applied to elucidate the membrane topology of other pore-forming RTX toxins. This is particularly important, as it does not currently seem feasible to obtain the 3D structure of any RTX toxin in the membrane using crystallographic and/or cryo-EM methods.

CRediT authorship contribution statement

Eliska Ruzickova: Writing – review & editing, Visualization, Validation, Methodology, Investigation, Formal analysis. **Michaela Lichvarova:** Validation, Methodology, Investigation, Formal analysis. **Adriana Osickova:** Validation, Supervision, Methodology, Investigation, Formal analysis. **Katerina Filipi:** Validation, Methodology, Investigation, Formal analysis. **David Jurnecka:** Validation, Methodology, Investigation, Formal analysis, Data curation. **Humaira Khaliq:** Validation, Methodology, Investigation, Formal analysis. **Carlos Espinosa-Vinals:** Validation, Methodology, Investigation, Formal analysis. **Petr Pompach:** Validation, Methodology, Investigation, Data curation. **Jiri Masin:** Validation, Methodology, Investigation. **Radim Osicka:** Writing – review & editing, Writing – original draft, Visualization, Validation, Supervision, Methodology, Investigation, Funding acquisition, Conceptualization.

Declaration of competing interest

The authors declare that they have no known competing financial interests or personal relationships that could have appeared to influence the work reported in this paper.

Acknowledgements

This work was supported by grant 22-15825S from the Czech Science Foundation (GACR) and by project LM2023053 (Czech National Node to the European Infrastructure for Translational Medicine) from The Ministry of Education, Youth and Sports of the Czech Republic. We acknowledge Structural mass Spectrometry Core Facility of CIISB, Instruct-CZ Centre, supported by The Ministry of Education, Youth and Sports of the Czech Republic (LM2023042) and European Regional Development Fund-Project "UP CIISB" (No. CZ.02.1.01/0.0/0.0/18_046/0015974). We also acknowledge support from Talking microbes - understanding microbial interactions within One Health framework (CZ.02.01.01/00/22_008/0004597). We would like to thank Sona Kozubova and Waheed Ur Rahman for their excellent technical assistance.

Appendix A. Supplementary data

Supplementary data to this article can be found online at https://doi.org/10.1016/j.ijbiomac.2024.137604.

Data availability

Data will be made available on request.

References

[1] S.D. Henriksen, K. Bovre, *Moraxella kingii* sp.nov., a haemolytic, saccharolytic species of the genus Moraxella, J. Gen. Microbiol. 51 (3) (1968) 377–385.
[2] P. Yagupsky, *Kingella kingae*: from medical rarity to an emerging paediatric pathogen, Lancet Infect. Dis. 4 (6) (2004) 358–367.
[3] P. Yagupsky, E. Porsch, J.W. St Geme 3rd, *Kingella kingae*: an emerging pathogen in young children, Pediatrics 127 (3) (2011) 557–565.
[4] V.L. Munoz, E.A. Porsch, J.W. St Geme, 3rd, Virulence determinants of the emerging pathogen *Kingella kingae*, Curr. Opin. Microbiol. 54 (2020) 37–42.
[5] C. Gouveia, M. Duarte, S. Norte, J. Arcangelo, M. Pinto, C. Correia, M.J. Simoes, H. Canhao, D. Tavares, *Kingella kingae* displaced *S. aureus* as the most common cause of acute septic arthritis in children of all ages, Pediatr. Infect. Dis. J. 40 (7) (2021) 623–627.
[6] P. Yagupsky, *Kingella kingae*: carriage, transmission, and disease, Clin. Microbiol. Rev. 28 (1) (2015) 54–79.
[7] A. Slonim, M. Steiner, P. Yagupsky, Immune response to invasive *Kingella kingae* infections, age-related incidence of disease, and levels of antibody to outer-membrane proteins, Clin. Infect. Dis. 37 (4) (2003) 521–527.
[8] A. Gene, J.J. Garcia-Garcia, P. Sala, M. Sierra, R. Huguet, Enhanced culture detection of *Kingella kingae*, a pathogen of increasing clinical importance in pediatrics, Pediatr. Infect. Dis. J. 23 (9) (2004) 886–888.
[9] D. Ceroni, V. Dubois-Ferriere, A. Cherkaoui, R. Gesuele, C. Combescure, L. Lamah, S. Manzano, J. Hibbs, J. Schrenzel, Detection of *Kingella kingae* osteoarticular infections in children by oropharyngeal swab PCR, Pediatrics 131 (1) (2013) e230–e235.
[10] G. Syridou, P. Giannopoulou, N. Charalampaki, J. Papaparaskevas, P. Korovessi, S. Papagianni, A. Tsakris, E. Trikka-Grafakou, Invasive infection from *Kingella kingae*: not only arthritis, IDCases 20 (2020) e00732.
[11] T.E. Kehl-Fie, J.W. St Geme 3rd, Identification and characterization of an RTX toxin in the emerging pathogen *Kingella kingae*, J. Bacteriol. 189 (2) (2007) 430–436.
[12] T.E. Kehl-Fie, S.E. Miller, J.W. St Geme 3rd, *Kingella kingae* expresses type IV pili that mediate adherence to respiratory epithelial and synovial cells, J. Bacteriol. 190 (21) (2008) 7157–7163.
[13] E.A. Porsch, T.E. Kehl-Fie, J.W. St Geme 3rd, Modulation of *Kingella kingae* adherence to human epithelial cells by type IV Pili, capsule, and a novel trimeric autotransporter, mBio 3 (5) (2012) e00372-12.
[14] K.F. Starr, E.A. Porsch, C. Heiss, I. Black, P. Azadi, J.W. St Geme 3rd, Characterization of the *Kingella kingae* polysaccharide capsule and exopolysaccharide, PLoS One 8 (9) (2013) e75409.
[15] E.A. Porsch, *Kingella kingae* virulence factors and insights into pathogenicity, Microorganisms 10 (5) (2022) 997.
[16] K. Filipi, W.U. Rahman, A. Osickova, R. Osicka, *Kingella kingae* RtxA cytotoxin in the context of other RTX toxins, Microorganisms 10 (3) (2022) 518.
[17] I. Linhartova, L. Bumba, J. Masin, M. Basler, R. Osicka, J. Kamanova, K. Prochazkova, I. Adkins, J. Hejnova-Holubova, L. Sadilkova, J. Morova, P. Sebo, RTX proteins: a highly diverse family secreted by a common mechanism, FEMS Microbiol. Rev. 34 (6) (2010) 1076–1112.
[18] I. Linhartova, R. Osicka, L. Bumba, J. Masin, P. Sebo, RTX Toxins: A Review, Microbial Toxins, Toxinology ed, Springer, Dordrecht, the Netherlands, 2015.
[19] J. Jumper, R. Evans, A. Pritzel, T. Green, M. Figurnov, O. Ronneberger, K. Tunyasuvunakool, R. Bates, A. Zidek, A. Potapenko, A. Bridgland, C. Meyer, S.A. A. Kohl, A.J. Ballard, A. Cowie, B. Romera-Paredes, S. Nikolov, R. Jain, J. Adler, T. Back, S. Petersen, D. Reiman, E. Clancy, M. Zielinski, M. Steinegger, M. Pacholska, T. Berghammer, S. Bodenstein, D. Silver, O. Vinyals, A.W. Senior, K. Kavukcuoglu, P. Kohli, D. Hassabis, Highly accurate protein structure prediction with AlphaFold, Nature 596 (7873) (2021) 583–589.
[20] M. Varadi, S. Anyango, M. Deshpande, S. Nair, C. Natassia, G. Yordanova, D. Yuan, O. Stroe, G. Wood, A. Laydon, A. Zidek, T. Green, K. Tunyasuvunakool, S. Petersen, J. Jumper, E. Clancy, R. Green, A. Vora, M. Lutfi, M. Figurnov, A. Cowie, N. Hobbs, P. Kohli, G. Kleywegt, E. Birney, D. Hassabis, S. Velankar, AlphaFold Protein Structure Database: massively expanding the structural coverage of protein-sequence space with high-accuracy models, Nucleic Acids Res. 50 (D1) (2022) D439–D444.
[21] A. Osickova, N. Balashova, J. Masin, M. Sulc, J. Roderova, T. Wald, A.C. Brown, E. Koufos, E.H. Chang, A. Giannakakis, E.T. Lally, R. Osicka, Cytotoxic activity of *Kingella kingae* RtxA toxin depends on post-translational acylation of lysine residues and cholesterol binding, Emerg Microbes Infect 7 (1) (2018) 178.
[22] A. Osickova, H. Khaliq, J. Masin, D. Jurnecka, A. Sukova, R. Fiser, J. Holubova, O. Stanek, P. Sebo, R. Osicka, Acyltransferase-mediated selection of the length of the fatty acyl chain and of the acylation site governs activation of bacterial RTX toxins, J. Biol. Chem. 295 (28) (2020) 9268–9280.
[23] W.U. Rahman, A. Osickova, N. Klimova, J. Lora, N. Balashova, R. Osicka, Binding of *Kingella kingae* RtxA toxin depends on cell surface oligosaccharides, but not on beta2 integrins, Int. J. Mol. Sci. 21 (23) (2020) 9092.
[24] W.U. Rahman, R. Fiser, R. Osicka, *Kingella kingae* RtxA toxin interacts with sialylated gangliosides, Microb. Pathog. 181 (2023) 106200.
[25] I. Bárcena-Uribarri, R. Benz, M. Winterhalter, E. Zakharian, N. Balashova, Pore forming activity of the potent RTX-toxin produced by pediatric pathogen *Kingella kingae*: characterization and comparison to other RTX-family members, Biochim. Biophys. Acta 1848 (7) (2015) 1536–1544.
[26] A.I. Pesce Viglietti, F.A. Sviercz, C.A.M. Lopez, R.N. Freiberger, J. Quarleri, M. V. Delpino, Proinflammatory microenvironment during *Kingella kingae* infection modulates osteoclastogenesis, Front. Immunol. 12 (2021) 757827.
[27] P. Lehours, A.M. Freydiere, O. Richer, C. Burucoa, S. Boisset, P. Lanotte, M. F. Prere, A. Ferroni, C. Lafuente, F. Vandenesch, F. Megraud, A. Menard, The *rtxA* toxin gene of *Kingella kingae*: a pertinent target for molecular diagnosis of osteoarticular infections, J. Clin. Microbiol. 49 (4) (2011) 1245–1250.
[28] U. Amit, N. Porat, R. Basmaci, P. Bidet, S. Bonacorsi, R. Dagan, P. Yagupsky, Genotyping of invasive *Kingella kingae* isolates reveals predominant clones and association with specific clinical syndromes, Clin. Infect. Dis. 55 (8) (2012) 1074–1079.
[29] R. Basmaci, P. Yagupsky, B. Ilharreborde, K. Guyot, N. Porat, M. Chomton, J. M. Thiberge, K. Mazda, E. Bingen, S. Bonacorsi, P. Bidet, Multilocus sequence typing and rtxA toxin gene sequencing analysis of *Kingella kingae* isolates demonstrates genetic diversity and international clones, PLoS One 7 (5) (2012) e38078.
[30] D.W. Chang, Y.A. Nudell, J. Lau, E. Zakharian, N.V. Balashova, RTX toxin plays a key role in *Kingella kingae* virulence in an infant rat model, Infect. Immun. 82 (6) (2014) 2318–2328.
[31] D.P. Morreale, E.A. Porsch, B.K. Kern, J.W. St Geme 3rd, P.J. Planet, Acquisition, co-option, and duplication of the rtx toxin system and the emergence of virulence in *Kingella*, Nat. Commun. 14 (1) (2023) 4281.
[32] F. Khan, M. He, M.J. Taussig, Double-hexahistidine tag with high-affinity binding for protein immobilization, purification, and detection on ni-nitrilotriacetic acid surfaces, Anal. Chem. 78 (9) (2006) 3072–3079.
[33] J.R. Wisniewski, A. Zougman, N. Nagaraj, M. Mann, Universal sample preparation method for proteome analysis, Nat. Methods 6 (5) (2009) 359–362.
[34] R. Benz, K. Janko, W. Boos, P. Lauger, Formation of large, ion-permeable membrane channels by the matrix protein (porin) of *Escherichia coli*, Biochim. Biophys. Acta 511 (3) (1978) 305–319.
[35] C. Nicolai, F. Sachs, Solving ion channel kinetics with the QuB software, Biophys. Rev. Lett. 08 (03) (2013) 191–211.
[36] A. Ludwig, A. Schmid, R. Benz, W. Goebel, Mutations affecting pore formation by haemolysin from *Escherichia coli*, Mol. Gen. Genet. 226 (1–2) (1991) 198–208.
[37] M.C. Gray, S.J. Lee, L.S. Gray, F.R. Zaretzky, A.S. Otero, G. Szabo, E.L. Hewlett, Translocation-specific conformation of adenylate cyclase toxin from *Bordetella pertussis* inhibits toxin-mediated hemolysis, J. Bacteriol. 183 (20) (2001) 5904–5910.
[38] J. Masin, R. Fiser, I. Linhartova, R. Osicka, L. Bumba, E.L. Hewlett, R. Benz, P. Sebo, Differences in purinergic amplification of osmotic cell lysis by the pore-forming RTX toxins *Bordetella pertussis* CyaA and *Actinobacillus pleuropneumoniae* ApxIA: the role of pore size, Infect. Immun. 81 (12) (2013) 4571–4582.
[39] J. Masin, A. Osickova, A. Sukova, R. Fiser, P. Halada, L. Bumba, I. Linhartova, R. Osicka, P. Sebo, Negatively charged residues of the segment linking the enzyme and cytolysin moieties restrict the membrane-permeabilizing capacity of adenylate cyclase toxin, Sci. Rep. 6 (2016) 29137.
[40] J.A. Killian, G. von Heijne, How proteins adapt to a membrane-water interface, Trends Biochem. Sci. 25 (9) (2000) 429–434.
[41] C. Hyland, L. Vuillard, C. Hughes, V. Koronakis, Membrane interaction of *Escherichia coli* hemolysin: flotation and insertion-dependent labeling by phospholipid vesicles, J. Bacteriol. 183 (18) (2001) 5364–5370.
[42] A. Valeva, I. Siegel, M. Wylenzek, T.M. Wassenaar, S. Weis, N. Heinz, R. Schmitt, C. Fischer, R. Reinartz, S. Bhakdi, I. Walev, Putative identification of an amphipathic alpha-helical sequence in hemolysin of *Escherichia coli* (HlyA) involved in transmembrane pore formation, Biol. Chem. 389 (9) (2008) 1201–1207.

[43] S. Bhakdi, N. Mackman, J.M. Nicaud, I.B. Holland, *Escherichia coli* hemolysin may damage target cell membranes by generating transmembrane pores, Infect. Immun. 52 (1) (1986) 63–69.
[44] R. Benz, E. Maier, D. Ladant, A. Ullmann, P. Sebo, Adenylate cyclase toxin (CyaA) of *Bordetella pertussis*. Evidence for the formation of small ion-permeable channels and comparison with HlyA of *Escherichia coli*, J. Biol. Chem. 269 (44) (1994) 27231–27239.
[45] A. Osickova, R. Osicka, E. Maier, R. Benz, P. Sebo, An amphipathic alpha-helix including glutamates 509 and 516 is crucial for membrane translocation of adenylate cyclase toxin and modulates formation and cation selectivity of its membrane channels, J. Biol. Chem. 274 (53) (1999) 37644–37650.
[46] M. Basler, O. Knapp, J. Masin, R. Fiser, E. Maier, R. Benz, P. Sebo, R. Osicka, Segments crucial for membrane translocation and pore-forming activity of *Bordetella* adenylate cyclase toxin, J. Biol. Chem. 282 (17) (2007) 12419–12429.
[47] J. Masin, J. Roderova, A. Osickova, P. Novak, L. Bumba, R. Fiser, P. Sebo, R. Osicka, The conserved tyrosine residue 940 plays a key structural role in membrane interaction of *Bordetella* adenylate cyclase toxin, Sci. Rep. 7 (1) (2017) 9330.
[48] J. Roderova, A. Osickova, A. Sukova, G. Mikusova, R. Fiser, P. Sebo, R. Osicka, J. Masin, Residues 529 to 549 participate in membrane penetration and pore-forming activity of the *Bordetella* adenylate cyclase toxin, Sci. Rep. 9 (1) (2019) 5758.
[49] D. Eisenberg, E. Schwarz, M. Komaromy, R. Wall, Analysis of membrane and surface protein sequences with the hydrophobic moment plot, J. Mol. Biol. 179 (1) (1984) 125–142.
[50] B. Powthongchin, C. Angsuthanasombat, Effects on haemolytic activity of single proline substitutions in the *Bordetella* pertussis CyaA pore-forming fragment, Arch. Microbiol. 191 (1) (2009) 1–9.
[51] S. Juntapremjit, N. Thamwiriyasati, C. Kurehong, P. Prangkio, L. Shank, B. Powthongchin, C. Angsuthanasombat, Functional importance of the Gly cluster in transmembrane helix 2 of the *Bordetella pertussis* CyaA-hemolysin: implications for toxin oligomerization and pore formation, Toxicon : official journal of the International Society on Toxinology 106 (2015) 14–19.
[52] U. Omasits, C.H. Ahrens, S. Muller, B. Wollscheid, Protter: interactive protein feature visualization and integration with experimental proteomic data, Bioinformatics 30 (6) (2014) 884–886.
[53] S.H. Feng, C.Q. Xia, P.D. Zhang, H.B. Shen, Ab-initio membrane protein amphipathic helix structure prediction using deep neural networks, IEEE/ACM Trans. Comput. Biol. Bioinform. 19 (2) (2022) 795–805.
[54] T. Nugent, D.T. Jones, Transmembrane protein topology prediction using support vector machines, BMC Bioinformatics 10 (2009) 159.
[55] H. Viklund, A. Elofsson, OCTOPUS: improving topology prediction by two-track ANN-based preference scores and an extended topological grammar, Bioinformatics 24 (15) (2008) 1662–1668.
[56] S.M. Reynolds, L. Kall, M.E. Riffle, J.A. Bilmes, W.S. Noble, Transmembrane topology and signal peptide prediction using dynamic bayesian networks, PLoS Comput. Biol. 4 (11) (2008) e1000213.
[57] L. Kall, A. Krogh, E.L. Sonnhammer, An HMM posterior decoder for sequence feature prediction that includes homology information, Bioinformatics 21 (Suppl. 1) (2005) i251–i257.
[58] H. Viklund, A. Elofsson, Best alpha-helical transmembrane protein topology predictions are achieved using hidden Markov models and evolutionary information, Protein Sci. 13 (7) (2004) 1908–1917.
[59] A. Rose, S. Lorenzen, A. Goede, B. Gruening, P.W. Hildebrand, RHYTHM—a server to predict the orientation of transmembrane helices in channels and membrane-coils, Nucleic Acids Res. 37 (Web Server issue) (2009) W575–W580.
[60] D. Juretic, L. Zoranic, D. Zucic, Basic charge clusters and predictions of membrane protein topology, J. Chem. Inf. Comput. Sci. 42 (3) (2002) 620–632.
[61] A. Bernsel, H. Viklund, J. Falk, E. Lindahl, G. von Heijne, A. Elofsson, Prediction of membrane-protein topology from first principles, Proc. Natl. Acad. Sci. USA 105 (20) (2008) 7177–7181.
[62] M. Bernhofer, C. Dallago, T. Karl, V. Satagopam, M. Heinzinger, M. Littmann, T. Olenyi, J. Qiu, K. Schutze, G. Yachdav, H. Ashkenazy, N. Ben-Tal, Y. Bromberg, T. Goldberg, L. Kajan, S. O'Donoghue, C. Sander, A. Schafferhans, A. Schlessinger, G. Vriend, M. Mirdita, P. Gawron, W. Gu, Y. Jarosz, C. Trefois, M. Steinegger, R. Schneider, B. Rost, PredictProtein - predicting protein structure and function for 29 years, Nucleic Acids Res. 49 (W1) (2021) W535–W540.
[63] K. Hofmann, W. Stoffel, TMbase - a database of membrane spanning proteins segments, Biol. Chem. Hoppe Seyler 374 (1–6) (1993) 166.
[64] A. Bernsel, H. Viklund, A. Hennerdal, A. Elofsson, TOPCONS: consensus prediction of membrane protein topology, Nucleic Acids Res. 37 (Web Server issue) (2009) W465–W468.